Journal of Metals, Materials and Minerals, 37(1), e2616, 2027

Enhancing superhydrophobicity of paper via gas-phase silylation using hexadecyltrimethoxysilane and titanium(IV) isopropoxide

Kamonwan PACAPHOL[1,2,3], Patcharawarin SATHAPORNWAJANA[1], and Kuntinee SUVARNAKICH[1,2,*]

[1] *Pulp, Paper and Packaging Technology Program, Faculty of Science, Chulalongkorn University, Bangkok, 10330, Thailand*
[2] *Department of Imaging and Printing Technology, Faculty of Science, Chulalongkorn University, Bangkok, 10330, Thailand*
[3] *Center of Excellence in Responsive Wearable Materials, Faculty of Science, Chulalongkorn University, Bangkok, 10330, Thailand*

***Corresponding author e-mail**: kuntinee.s@chula.ac.th

Received date:
26 December 2025
Revised date:
21 July 2026
Accepted date:
11 September 2026

Keywords:
Water-resistance paper;
Chemical vapor deposition;
Superhydrophobicity;
Silylation;
Silane

Abstract

The shift toward paper-based packaging is driven by concerns over the non-biodegradability and environmental impact of plastics. Although paper is biodegradable, its poor water resistance limits broader applications. This study aimed to improve the water resistance of paper through chemical vapor deposition (CVD) silylation using different volumes of hexadecyltrimethoxysilane (HDTMS) in the gas phase, which enables deeper penetration into the paper structure than conventional surface coatings. Titanium (IV) isopropoxide (TTIP) was applied as a catalytic primer via spray coating at various concentrations. The results showed that HDTMS alone, at 28 mL·m^{-2}, produced a hydrophobic surface with a water contact angle of 115° on both sides of the paper. Incorporating 10% v/v TTIP and applying a 30 min vapor deposition generated a superhydrophobic surface, increasing water contact angle from 0° (untreated) to 151° and reducing the Cobb value from 435 g·m^{-2} to 17 g·m^{-2} on both sides of the paper. Meanwhile, the treated paper maintained water vapor and oxygen permeability comparable to the untreated sample. FT-IR, XRF, AFM, and SEM analyses confirmed successful silylation. Overall, the gas-phase silylation approach effectively enhanced water resistance while maintaining vapor permeability, showing promise for developing breathable waterproof paper for medical, healthcare, and fresh-produce packaging applications.

1. Introduction

Plastics are widely used as packaging materials due to their desirable properties, including resistance to thermal, water, and external forces, as well as their safety for food contact. However, plastics are non-biodegradable and gradually fragment into microplastics that contaminate the environment [1]. Global plastic production exceeds one hundred million tons annually, resulting in a substantial accumulation of plastic waste and severe environmental concerns [2]. Consequently, paper has emerged as a sustainable alternative because it is biodegradable, recyclable, and derived from renewable resources [3]. Nevertheless, paper still presents several limitations when employed as a packaging material, particularly poor water resistance. This poor resistance arises from the hydrophilic nature of cellulose fibers, which contain abundant hydroxyl groups (–OH) [4].

Traditionally, the improvement of paper's water resistance has relied on synthetic polymer coatings, such as acrylics, which are inexpensive and easy to process. Common coatings used in the paper packaging industry have traditionally included petroleum-based synthetic polymers such as styrene-butadiene latex (SB latex), styrene-acrylic latex (SA latex), and polyvinyl acetate (PVAc) [5]. Among these, SB latex is the most prevalent, accounting for approximately 75% of all latex types used for coating conventional paper and paperboard [6]. Although these polymers are easily manufactured, readily available, and inexpensive, their petroleum origin raises environmental concerns related to non-degradability and greenhouse gas emissions [7]. More recently, attention has shifted toward the development of environmentally friendly alternatives, including natural-based coatings such as modified starches and waxes, to enhance the hydrophobicity and sustainability of paper materials.

Cationic starch has gained increasing attention in the packaging industry. However, its high content of hydroxyl groups renders it hydrophilic, leading to high water absorption. Therefore, starch modification is necessary—such as depositing long hydro-carbon chains onto its helical structure or incorporating oils or waxes into the starch suspension—to improve its hydrophobicity [8]. Carnauba wax, extracted from the Brazilian palm tree, exhibits strong hydrophobicity and is used to enhance the moisture barrier of paper coatings. Nevertheless, it can decrease paper strength after drying, and its relatively low melting point (82°C) can cause softening or melting during coating, paper production, or transportation [9]. Enhancing paper hydrophobicity can also be achieved through surface modification with silane compounds. Silanes can form covalent bonds with hydroxyl groups on the cellulose surface, introducing non-polar functional groups that lower surface energy. Commonly used silanes include triethoxymethylsilane (TEMS), tetraethoxysilane (TEOS), and polydimethylsiloxane (PDMS). Jing *et al.* [10] reported that coating paper with PDMS and chitosan produced water- and oil-resistant packaging

with a hydrophobic contact angle of 138°. Although these materials are environmentally friendly, the achieved hydrophobicity may still be insufficient for certain applications.

Hexadecyltrimethoxysilane (HDTMS) is another widely studied silane used to reduce surface energy and improve water repellency [11]. Seth *et al.* demonstrated that combining HDTMS with nickel nitrate hexahydrate via a dip-coating method enhanced the water resistance of cotton fabric, achieving a water contact angle of 162° and a sliding angle of 8° [12]. Similarly, Srishti and Kumar coated jute fabric with HDTMS and TiO_2 nanoparticles, resulting in a water contact angle of 161.5° [13]. The enhanced hydrophobicity arises from the long hydrocarbon chains of silane created on the cellulose surface, which reduces surface polarity and increases surface roughness [14]. Despite these promising results, conventional coating techniques still face challenges, including non-uniform coating distribution, enhanced water resistance only on the coated side of the paper, and the short pot life of silane-based mixtures due to their high sensitivity to hydrolysis reaction [15].

Chemical vapor deposition (CVD) represents another alternative approach for enhancing water resistance of paper. Moreover, this technique allows the coating or deposition of substances that are incompatible with direct solvent contact, including those that are sensitive to water or hydrolysis reactions, onto the desired substrates [13]. Although CVD has been extensively employed in the semiconductor industry for depositing inorganic materials, it has recently been adapted for coating polymeric substrates [15]. The CVD method can impart superhydrophobic properties using only a small quantity of precursor solution to generate the vapor phase [16,17], and it can be further developed from the laboratory scale to industrial production.

Gas-phase silylation via the CVD has been investigated in previous studies, some of which have demonstrated the feasibility of gas-phase organosilane modification of cellulose-based materials. However, most of these studies have focused on non-paper materials, such as wood, textiles, and aerogels, and have required relatively long treatment times. For instance, Rafieian *et al.* [18] modified cellulose nanofiber (CNF) aerogels with HDTMS by CVD at 155°C for 1 h, primarily for oil adsorption and oil/water separation. Similarly, Yue *et al.* [19] investigated gas-phase silylation of wood surfaces using hexamethyldisilazane (HMDS), achieving a superhydrophobic surface with a water contact angle of 157.6° after a 6 h reactions. Cao *et al.* [20] applied HDTMS-CVD to cellulose-, holocellulose-, and lignocellulose-based aerogels using reaction times of 2 h to 6 h, with optimized conditions of 100°C for 4 h for cellulose and holocellulose aerogels and 100°C for 2 h for the all-component biomass aerogel. Gas-phase modification of conventional paper has also been reported by Yu *et al.* [21]; however, their work employed organosilanes such as perfluorooctyltriethoxysilane (PFTS), HMDS, methyltrimethoxysilane (MTMS), and n-dodecyltrimethoxysilane (n-DDTS) rather than HDTMS, and hydrophobic modification of PFTS-treated filter paper approached its maximum after approximately 4 h of treatment. In contrast, the present study introduces Titanium(IV) isopropoxide (TTIP) as a catalytic primer prior to HDTMS gas-phase silylation onto paper. The Ti–OR species in TTIP are proposed to promote HDTMS condensation while simultaneously providing interfacial coupling sites between the hydroxyl-rich cellulose surface and the HDTMS-hydrolyzed siloxane layer (see Section 3.1 for the proposed mechanism). Thus, the novelty of this work lies not simply in the use of HDTMS-CVD, but in the TTIP-assisted catalytic-primer strategy designed to accelerate the silylation reaction, enhance interfacial bonding, and reduce the treatment time required to obtain superhydrophobic paper.

In this study, the concept of gas-phase silylation was employed, enabling the vapor to penetrate the fibrous network of paper and react thoroughly with the hydroxyl groups on the cellulose surface through the formation of covalent bonds. The objective is to fabricate superhydrophobic paper by investigating the effects of gas-phase silylation conditions and the amount of HDTMS, while employing titanium (IV) isopropoxide (TTIP) as a catalyst to reduce the reaction time and enhance bonding efficiency on the organic surface of cellulose, with which silane normally reacts less effectively than with inorganic surfaces. This research aims to determine the optimal conditions and proportions of HDTMS and TTIP for creating a superhydrophobic surface on high-absorbent paper, based on the results of water absorption tests that reflect both surface and bulk properties. The findings are intended to provide fundamental insights for developing superhydrophobic paper through a novel approach applicable to paper packaging and related applications. The experimental layout is illustrated in Figure 1.

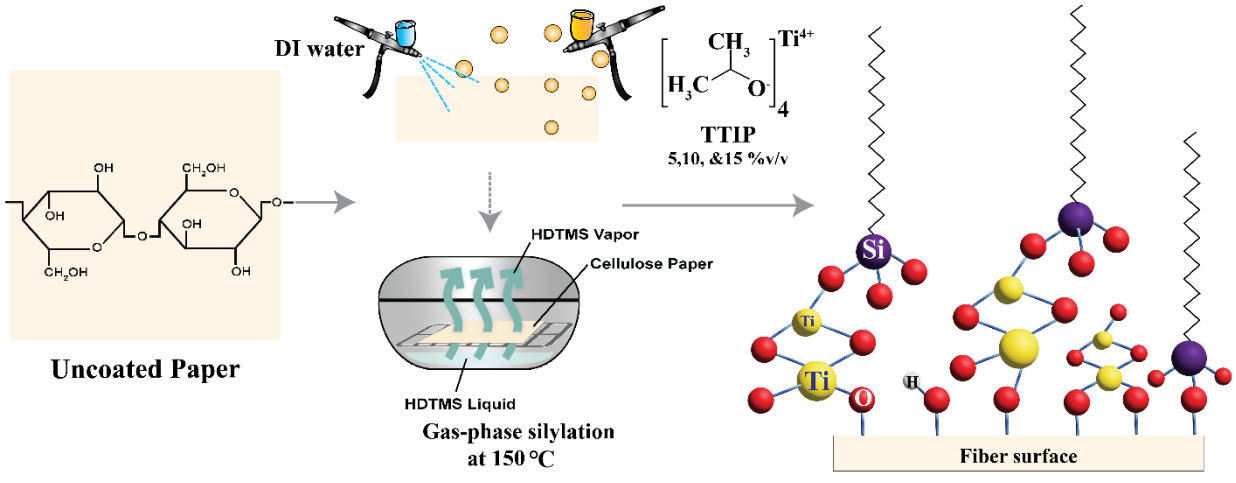


Figure 1. Experimental layout of gas-phase silylation using HDTMS and TTIP.

2. Experimental

2.1 Materials and chemicals

HDTMS, 85% to 95% purity, was supplied by BRB International (Ittervoort, the Netherlands). TTIP, ethanol, and acetic acid were supplied by Sigma Aldrich. Standard blotting paper sheets (420 cm^2, 260 ± 5 $g{\cdot}m^{-2}$, 500 ± 10 μm thick) were supplied by Certified Lab Consulting. A stainless-steel container with a diameter of 12 cm and a height of 5 cm, having an area of approximately 114 cm^2, was used as a vapor deposition chamber. A stainless-steel grid with a diameter of 7 cm and a height of 0.5 cm was used as a supporting base for placing the paper sample inside the container. The container was sealed using a heat-resistant polyamide tape (20 mm wide, 50 μm thick).

2.2 Paper preparation

The blotting paper (basis weight 260 ± 5 $g{\cdot}m^{-2}$, thickness 500 ± 10 μm) was used in this experiment. Blotting paper was selected because it represents unsized and uncoated paper. The sheets were cut into 6 cm × 6 cm pieces and conditioned in a standard atmosphere according to TAPPI T402 sp-08.

2.3 Determination of the optimal amount of HDTMS for chemical vapor deposition

The gas-phase silylation procedure was adapted from the method of Yu *et al.* [21]. Different amounts of HDTMS of 0.1 mL, 0.5 mL, and 1.0 mL, designated as 0.1H, 0.5H, and 1H, were tested on paper samples with an area of 6 cm × 6 cm paper surface. The HDTMS liquid was poured into a stainless-steel container equipped with a wire mesh at the center, while the paper sample was positioned on a grid located 0.5 cm above the bottom of the container. The container was then tightly sealed with heat-resistant polyamide tape and placed in an oven at 150°C for 60 min to allow gas-phase silylation to occur. The reaction temperature of 150°C was selected based on preliminary tests (see Table S1 in the Supplementary Data file). Each condition was prepared in triplicate.

2.4 Determination of the optimal concentration of TTIP and the vapor deposition time

Different TTIP concentrations of 5%, 10%, and 15% v/v in ethanol were prepared at room temperature. Then, 1 mL of the TTIP solution was loaded into an airbrush spray and evenly applied to both sides of the blotting paper, each side having a surface area of 36 cm^2. Then, the gas-phase silylation reaction was carried out using the selected amount of HDTMS, following the chemical vapor deposition procedure described in Section 2.3. These samples were designated according to different TTIP concentrations of 5%, 10%, and 15% (v/v) as 0.1H+5T, 0.1H+10T, and 0.1H+15T, respectively. After determining the optimal amounts of HDTMS and TTIP, the vapor deposition time was varied to identify the shortest duration required to achieve superhydrophobicity on paper, with controlled oven times of 10 min, 30 min, and 60 min under a maintained temperature of 150°C.

2.5 Characterization and property tests

2.5.1 Morphology

For morphological characterization, the paper samples (1 cm × 1 cm) were sputter-coated with a thin gold layer to enhance electrical conductivity. The samples were subsequently examined using a Scanning Electron Microscope (SEM; JSM-IT800, JEOL, Peabody, MA, USA) operated at 15 kV.

2.5.2 Chemical structure

Functional groups of untreated and treated papers were characterized using a Fourier transform infrared spectroscopy (FT-IR) with an integrated iD7 ATR accessory (Nicolet iS5, Thermo Scientific Waltham, MA, USA) at 64 scans with a spectra resolution of 4 cm^{-1} in the wavenumber range of 500 cm^{-1} to 4000 cm^{-1}.

2.5.3 Elemental composition

The elemental composition on the surfaces of untreated and treated paper samples was investigated using a micro-X-ray fluorescence spectrometer (Micro-XRF: M4 Tornado, Bruker Artax, Karlsruhe, Germany). The instrument was equipped with a Rhodium (Rh) target X-ray tube and a Silicon Drift Detector. The operating parameters were set to a high voltage of 50 kV and an anode current of 599 μA, with no filter applied. Elemental maps were acquired using a 20 μm spot size, a pixel size (step size) of 50 μm, and a dwell time of 20 ms/pixel.

2.5.4 Water absorption and water sliding angle as a surface properties

The surface absorption of the samples was evaluated by measuring the static water contact angle using the sessile drop method. The analysis was performed with a contact angle goniometer (OCA-15EC, DataPhysics Instruments, Filderstadt, Germany), following the ASTM D7334–08. A 3 μL droplet of distilled water was placed onto the sample surface, and the water contact angle was recorded at the 20 s time point after the initial contact. To ensure statistical reliability and evaluate surface homogeneity, at least ten measurements were taken at different locations on each sample. The final water contact angle value reported represents an average of five replicates.

The water sliding angle (SA) of the modified paper was measured using a contact angle meter (SL200KS, KINO Industry, GA, USA). A 10 μL droplet of deionized water was placed on the sample surface, after which the sample stage was gradually tilted. The inclination angle at which the droplet began to slide was recorded as the SA.

2.5.5 Water absorption as a bulk property

The Cobb test follows from the TAPPI T441 om-24 standard method using an inner stainless-steel ring with a diameter of 3.5 cm. The paper sample was cut into a circle with a diameter of 4 cm. Then, the stainless- steel ring was tightly fastened on the top of the water absorption apparatus to prevent water leakage. Distilled water was poured into the ring until it reached the notch mark at a height of

1 cm (test area = 10 cm^2). The timer was started immediately for 120 s as the water first contacted the paper during pouring. At the end of 120 s, the water was poured off, and the excess water was removed from the paper sample by rolling the metal roller once back and forth over the blotting paper placed on top of the specimen. Finally, the paper sample was weighed to calculate Cobb values according to Equation (1) [22].

$$\text{Cobb value } (g \cdot m^{-2}) = (w_2 - w_1) \times 1000 \quad (1)$$

Where w_1 and w_2 are the sample weights before and after the test, respectively. A factor of 1000 was derived from the test area (10 cm^2).

2.5.6 Surface roughness

Atomic force microscopy (AFM) was employed to characterize the surface roughness of untreated and treated paper samples using an XploRA Nano system (HORIBA France SAS, France). Surface topography images were collected over a scanning area of 5 μm × 5 μm, while the root mean square roughness (Rq) was calculated from selected 1 μm × 1 μm regions. Since gas-phase silylation modifies the surfaces of individual fibers through surface reactions rather than forming a continuous coating layer, the Rq values were determined from selected regions on individual fiber surfaces. Measurements were conducted at three different regions on each specimen as replicates to account for surface heterogeneity.

2.5.7 Water vapor transmission rate

The Water vapor transmission rate (WVTR) was measured according to ASTM E96-24 to evaluate the water vapor barrier property of the treated paper. The water method was employed using 40 mL of distilled water under controlled conditions of 23 ± 1.0°C and 50 ± 2.0% relative humidity. The WVTR in grams per 24 h and per square meter is calculated by using the following Equation: (2), and the average value from three samples was reported [23].

$$\text{WVTR } (g \cdot m^{-2} \cdot day^{-1}) = \frac{G}{A \times T} \quad (2)$$

where G is the weight change (g), T is the test time (24 h), and A is the sample area (m^2).

2.5.8 Oxygen transmission rate

The oxygen transmission rate (OTR) of untreated and treated paper samples was determined using an oxygen permeation analyzer (OX-TRAN 2/22L, AMETEK MOCON, Minneapolis, MN, USA) in accordance with ASTM D3985. Measurements were conducted at 23°C under a pressure of 101 kPa with 0% relative humidity (RH) for both the permeant and carrier gases. The paper thickness was 500 μm, and the effective test area was 5.64 cm^2. All measurements were performed in triplicate.

2.5.9 Color difference between untreated and treated papers

The colorimetric properties of the sample surfaces were analyzed using a spectrophotometer (CM-700, Konica Minolta, Japan) equipped with an 8 mm measurement aperture. All measurements were performed under a D65 standard illuminant and a 10° standard observer. The surface color was expressed in terms of the CIELAB color space coordinates (L*, a*, and b*). The total color difference (ΔE*) between the untreated and treated samples was calculated according to Equation (3). Each ΔE* value represents the mean of five replicate measurements [24].

$$\Delta E^* = \sqrt{\left(L^*_{treated} - L^*_{untreated}\right)^2 + \left(a^*_{treated} - a^*_{untreated}\right)^2 + \left(b^*_{treated} - b^*_{untreated}\right)^2} \quad (3)$$

where L^* represents lightness coordinate; a^* represents red–green coordinate; and b^* represents yellow–blue coordinate.

2.5.10 Stability and durability of treated paper

The durability of surface hydrophobicity during prolonged storage was assessed by monitoring changes in the water contact angle. Measurements were conducted on untreated paper and the best-performing treated paper. The initial water contact angle values were measured immediately after sample preparation (day 0), and the measurements were repeated after 7 months of storage at 25 ± 2°C and 30 ± 5% RH. Water contact angle measurements were performed using a contact angle goniometer (PGX+, Rycobel, Belgium). For each measurement, a 5 μL droplet of deionized water was placed onto the sample surface, and the contact angle was recorded 60 s after droplet placement.

The environmental stability under application-relevant conditions of the treated paper was evaluated under freezing, dry-heat, and hot-humid conditions. Samples were stored at –18°C, heated at 90°C, or exposed to steam, while samples kept under ambient conditions served as the reference. After exposure for 2 h in each condition, water contact angle was measured to assess the stability of the treated surface under different environmental conditions.

Mechanical abrasion resistance was evaluated using a Rub Tester (Model 10–20, TMI, PA, USA); the test method was slightly adapted from ASTM D5264. Blotting paper was cut into strips measuring 2 in × 7 in. and used as the rubbing material. Treated paper specimens measuring 3 cm × 6 cm were affixed to 3 in × 5 in. paper sheets and mounted on the tester. The abrasion test was performed under a load of 1.8 kg at a rubbing speed of 85 cycles·min^{-1}. The specimens were subjected to 10, 30, and 50 rubbing cycles to evaluate the durability of the treated surface against mechanical abrasion. The durability of the surface treatment was subsequently evaluated by monitoring changes in water contact angle after the specified numbers of rubbing cycles.

The durability of the treated paper against peeling was evaluated using a tape-peel test based on ASTM D3359. Specimens measuring 3 cm × 6 cm were prepared for testing. A strip of transparent adhesive tape (Scotch™ 500, 3M, USA) was firmly pressed onto the treated surface to ensure uniform contact. The tape was then peeled back from the surface at an angle of 180° [25]. The peeling process was repeated at the same location for one, two, and three cycles. The durability of the treatment was subsequently evaluated by monitoring changes in water contact angle after each peeling cycle.

The household chemical resistance of untreated and treated paper samples was evaluated using green water-soluble dye, vegetable oil, vinegar (pH 2), baking soda solution (pH 9), milk, and cola. Each liquid

was applied to the sample surface and left for 30 min. Surface changes and liquid penetration were then visually assessed.

2.6 Statistical analysis

All experiments were performed at least triplicate, and the results are expressed as mean ± standard deviation (SD). To select the optimal treatment condition based on surface and bulk water-resistance properties, statistical differences among sample groups were analyzed using one-way ANOVA followed by Duncan's multiple range test with statistical significance set at $p < 0.05$.

3. Results and discussion

3.1 Morphology

The morphology of the paper samples was examined using a SEM, as shown in Figure 2. The untreated paper exhibited a porous fibrous network structure distributed throughout the surface at low magnification, while individual fibers displayed a naturally smooth surface at higher magnification (Figure 2(a–b)). After gas-phase silylation treatment with HDTMS (without TTIP) at different amounts (Figure 2(c–h)), the low magnification images of the treated paper still show this porous fibrous network structure without coating layer found, similar to the paper before treatment. However, when observing at a higher magnification (Figure 2(d,f,h), the morphological change of fibers was observed, where fine particles were found on fiber surface. This indicated that small molecules of HDTMS in gas phase permeated through individual fibers and interacted with the cellulose surface instead of generating the coating layer. Surprisingly, these treated samples with the porous network structure provided the remarkedly increase of the water contact angle from 0° to 142° in all treated amounts, even the lowest amount of HDTMS at 0.1 mL (0.1H sample). Therefore, the 0.1H sample was selected to be studied with TTIP catalyst for the reduction of vapor deposition time. The results of the treated paper prepared using HDTMS gas-phase silylation with a TTIP catalyst still exhibited a porous fibrous network structure at a low TTIP concentration of 5% v/v (Figure 2(i)). However, when observing the fiber surface at higher magnification (Figure 2(j)), a rough coating layer on the cellulose fibers was observed, and the water contact angle significantly increased compared to the silylation treatment without the TTIP catalyst. The surface roughness progressively increased with increasing TTIP concentration. When the concentration was increased to 10% v/v, aggregated particles began to appear, and a thicker, rough surface layer was found on the individual fibers, leading to an increase in the water contact angle from 149° to 151°. At a higher TTIP concentration of 15% v/v, the aggregated particles densely covered the fiber surfaces, and cracks were observed in the rough coating layer (Figure 2(m–n). These cracks indicated the excessive deposition of TTIP at 15% v/v; although the water contact angle further increased compared to the 10% v/v sample, this excessive deposition created defect points where powder-like particles detached from the surface under external forces. Thus, even though one-way ANOVA showed that the 15% v/v sample exhibited a significantly higher contact angle (Figure 2(m–n) than the 10% v/v sample (Figure 2 (k–l), the 10% v/v sample was selected for further experiments. Increasing the amount of HDTMS liquid in the gas-phase silylation container had no significant effect on the fibrous network structure or the water contact angle, as a certain amount of HDTMS liquid remained in the container. This indicates the benefit of using a low dosage in the gas-phase reaction due to the efficient diffusion of gas molecules. The formation of long hydrocarbon chains derived from HDTMS on the cellulose fibers was a key factor contributing to the increase in water contact angle, confirming the successful hydrophobic surface modification [26]. When TTIP was incorporated into the HDTMS system, in addition to its catalytic role, TiO_2 particles were formed through the hydrolysis and condensation of TTIP in the presence of moisture, and hydrolyzed Ti–OH species were also generated and could interact with silanol (Si–OH) groups of HDTMS. Non-uniformity of particle deposition was observed on the fiber surface in Figure 2 (c–h), in contrast to the more uniform particles and layer observed in Figure 2(i–l), implying that a primer layer of TTIP assisted in bonding HDTMS onto the cellulose surface.

TTIP was employed as a catalytic primer to facilitate the gas-phase silylation of cellulose with HDTMS. In its catalytic role, TTIP belongs to the titanium alkoxide family, in which the Ti(IV) center acts as a well-known Lewis acidic and highly susceptible to ligand-exchange reactions with oxygen-containing species. Upon spraying TTIP in ethanol onto the moistened paper, rapid partial hydrolysis is expected to generate Ti species containing both Ti–OH and residual Ti–OR groups. Because the treated paper was immediately subjected to CVD, Ti–OR groups remain available during HDTMS deposition. When HDTMS vapor reaches water retained by the moistened cellulose, partial hydrolysis generates reactive Si–OH species. The residual Ti–OR sites can rapidly undergo ligand exchange with these Si–OH species to form titanium–silanolate (Ti–O–Si) intermediates. These intermediates subsequently react with additional alkoxy/silanol-containing silane species to form Si–O–Si bonds while regenerating Ti–OR functionality, thereby providing an alternative catalytic pathway for siloxane condensation and accelerating network formation [27]. This interpretation is consistent with previous work reporting the ability of $Ti(OR)_4$ species to catalyze silanol condensation and with the formation of Ti–O–Si bonds during alkoxysilane hydrolysis–condensation on titanium-containing surfaces [28].

In parallel, partially hydrolyzed TTIP acts as a reactive interfacial primer between cellulose and HDTMS. Ti–OH species can react with the abundant C–OH groups of cellulose to form covalent bonds (C–O–Ti), leaving additional Ti–OH functionalities available for subsequent silane attachment [29]. This Ti-mediated pathway is important because silanol groups generally undergo more favorable condensation with hydroxylated inorganic surfaces than with the hydroxyl groups of organic cellulose. Therefore, the Ti–OH-containing interphase formed by TTIP provides more reactive, inorganic-like sites for subsequent condensation with HDTMS-derived Si–OH groups, facilitating the formation of Ti–O–Si bonds [30] and producing proposed Cellulose–O–Ti–O–Si–$C_{16}H_{33}$ linkages, while neighboring Si–OH species may undergo further Si–O–Si condensation. This proposed reaction is consistent with Rashid *et al.* [31], who identified Si–O–Ti and Si–O–Si bonds in TTIP-derived TiO_2/organosilane coatings on cotton cellulose, supporting the formation of these linkages on cellulose-based substrates. Figure 3 illustrates the proposed mechanism of TTIP-assisted HDTMS vapor deposition onto cellulose.

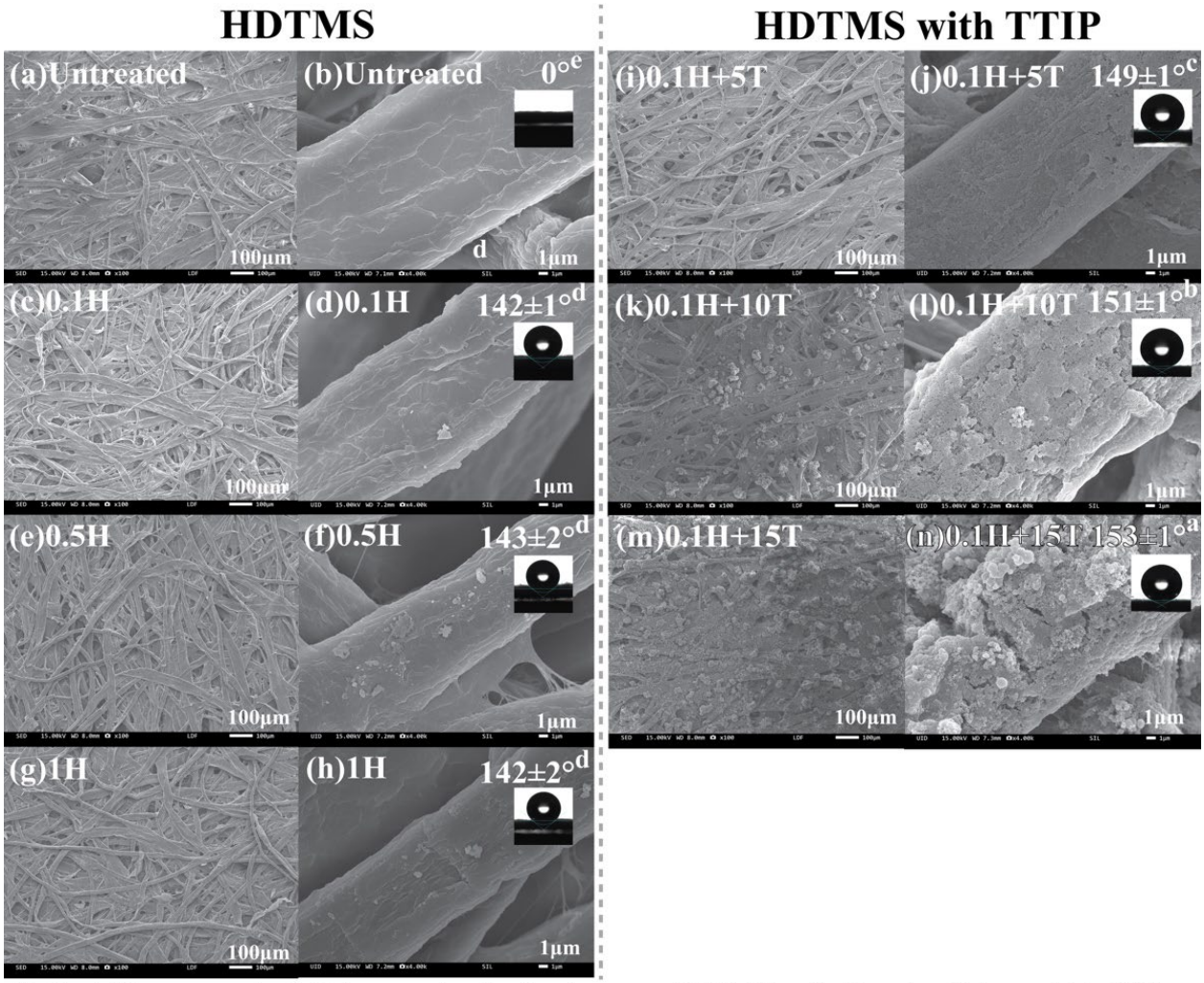


Figure 2. SEM images of the paper samples at 100x and 4000x magnifications: (a, b) untreated paper and treated papers with (c, d) 0.1H, (e, f) 0.5H, (g, h) 1.0H, (i, j) 0.1H+5T, (k, l) 0.1H+10T, and (m, n) 0.1H+15T.

Partial hydrolysis of TTIP (R = i-Pr) $Ti(OR)_4 + xH_2O \rightarrow Ti(OR)_{4-x}(OH)_x + xROH$ (1)*

TTIP-derived Ti species on cellulose $Cellulose{-}OH + Ti(OR)_{4-x}(OH)_x \rightarrow Cellulose{-}O{-}Ti(OR)_{3-x}(OH)_x + ROH$ (2)

Hydrolysis of HDTMS during CVD $C_{16}H_{33}Si(OCH_3)_3 + xH_2O \rightarrow C_{16}H_{33}Si{-}(OCH_3)_{3-x}(OH)_x + xCH_3OH$ (3)

TTIP-assisted grafting of HDTMS on cellulose $Cellulose{-}O{-}Ti{-}OH + HO{-}Si(C_{16}H_{33})(OCH_3)_2 \rightarrow Cellulose{-}O{-}Ti{-}O{-}Si(C_{16}H_{33})(OCH_3)_2 + H_2O$ (4)

* Partial hydrolysis of TTIP on the moistened cellulose is expected to generate a distribution of Ti species containing both residual Ti–OR groups (for catalytic function) and newly formed Ti–OH functionalities.

Figure 3. Proposed mechanism of TTIP-assisted HDTMS vapor deposition onto cellulose.

3.2 Chemical structure

Figure 4(a) shows the FT-IR spectra of the paper samples. The broad absorption band observed at 3290 cm^{-1} to 3330 cm^{-1} is associated with the stretching vibration of hydroxyl groups, which originates from the cellulose structure. The intensity of this band decreased after surface treatment, indicating a reduction in the number of accessible hydroxyl groups. The peaks appearing at around 2880 cm^{-1} and 1020 cm^{-1} correspond to the stretching vibrations of C–H and C–O–C groups, respectively, attributed to the anhydroglucose units in cellulose [32]. After gas-phase silylation with HDTMS and TTIP, two new peaks emerged at 2915 cm^{-1} and 2850 cm^{-1}, corresponding to the stretching vibrations of $–CH_2$ and $–CH_3$ groups. Additionally, the peak at 1470 cm^{-1} represents the bending vibration of the –CH group, confirming the presence of HDTMS functional groups. In the range of 400 cm^{-1} to 890 cm^{-1}, characteristic absorption bands of Ti–O and O–Ti–O were observed, which are typical of TiO_2 particles formed by the TTIP treatment [33]. For the sample treated with only 0.1H, the newly formed

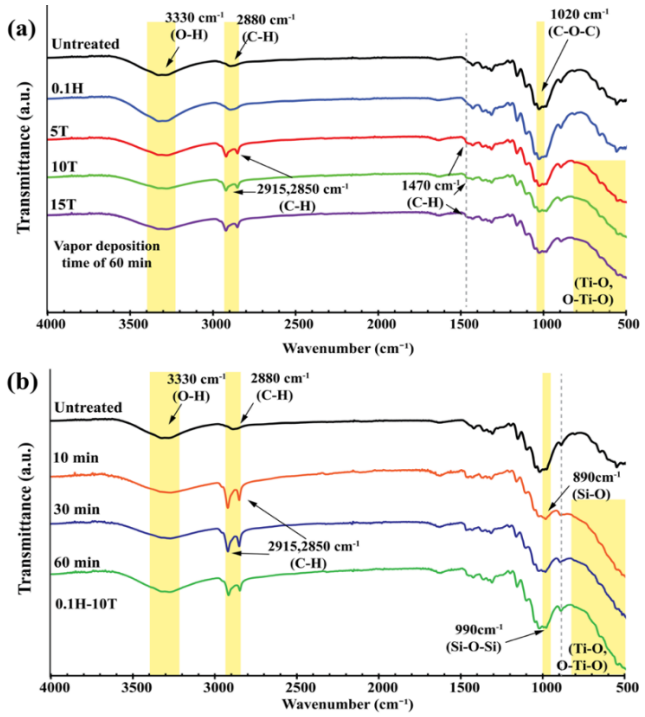


Figure 4. FT-IR spectra of untreated and HDTMS-treated paper with (a) different TTIP concentrations and (b) different vapor deposition times.

peaks were less prominent, likely due to the small HDTMS amount used and the surface sensitivity of the FT-IR technique. However, as shown in Figure 4(b), distinct peaks at around 890 cm^{-1} and 990 cm^{-1} were observed, corresponding to the stretching vibrations of Si–O and Si–O–Si bonds, respectively [34]. These peaks indicate the successful silylation reaction of HDTMS with TiO_2 and hydroxyl groups on the paper surface [35], although some overlap with other absorption bands was observed. All samples with different silylation durations (vapor deposition times) exhibited new characteristic functional groups compared to the untreated sample (0 min), confirming the successful incorporation of HDTMS and TTIP onto the paper surface. Surface wettability strongly influences liquid–solid interfacial interactions, particularly through changes in droplet spreading and effective contact area. Therefore, tailoring surface chemistry to control wettability is an important strategy for regulating the interaction between water droplets and solid surfaces [36].

3.3 Elemental composition

The elemental composition analysis of the untreated paper revealed Ca (80.4%) and Al (8.2%) as the major inorganic fillers typically found in paper materials. After gas-phase silylation with HDTMS (the 0.1H sample without TTIP), the surface Si content increased to 1.98%, while Al slightly decreased to 7.0%, indicating the presence of HDTMS molecules on the paper surface. When the paper was modified with HDTMS in the presence of TTIP solutions at various concentrations, 5%, 10%, and 15% v/v, Ti was detected on the surface at 69.1%, 73%, and 90.5%, respectively. The appearance of Ti originated from the hydrolysis and condensation of TTIP, which reacted with hydroxyl groups of cellulose fibers and also underwent self-crosslinking, especially at higher TTIP concentrations, as clearly shown by the aggregated particles in Figure 2(k). In addition, the Si content increased from 1.98% (in the untreated sample) to 12.8%, 18.2%, and 5.3% for the samples with increasing TTIP concentrations, respectively. The elevated Si content mainly resulted from the condensation reaction between HDTMS and TTIP, as well as the formation of covalent bonds between HDTMS and the hydroxyl groups of cellulose fibers. The trend of increasing Si content with higher TTIP concentration (at a constant HDTMS amount of 0.1 mL in the gas-phase silylation container) suggests an improved bonding capability, with TTIP functioning as a primer or coupling agent (see Figure 4(b)). However, at excessively high TTIP concentration (the 0.1H–15T sample), the Si percentage decreased due to the surface shielding effect caused by the large amount of Ti deposition.

In our study, the Si content was present at a lower percentage ratio compared to the coating material reported by Zhang *et al.* [37], who fabricated sericite–TiO_2/HDTMS superhydrophobic coatings and sprayed them onto glass substrates, obtaining Si and Ti ratios of 50.1% and 27.7%, respectively. This difference can be attributed to the use of HDTMS gas molecules in the vapor deposition process in our work, where a smaller amount of HDTMS was employed. Despite the lower reagent usage, a comparable water contact angle was achieved, demonstrating the efficiency of our method.

3.4 Water absorption: surface and bulk properties

3.4.1 Water contact angle and water sliding angle

The water contact angle measurements were conducted to evaluate the water resistance of the paper surfaces, as shown in Figure 5. The untreated paper exhibited a contact angle of 0° on both the front and back sides, indicating its hydrophilic nature. After gas-phase silylation with HDTMS (without TTIP), the 0.1H sample showed average contact angles of 142° and 140° for the front and back surfaces, respectively. When increasing the amount of HDTMS in the gas-phase silylation container, the 0.5H and 1H samples exhibited similar results, with average contact angles of approximately 140° to 143° on both sides

Table 1. Elemental concentration of treated and untreated paper samples using XRF.

Sample	Elemental concentration* [%]		
	Si	Ti	Ca
Untreated	n/a	n/a	80.4
0.1H	2.0	n/a	80.5
0.1H+5T	12.8	69.1	14.1
0.1H+10T	18.2	73.0	7.4
0.1H+15T	5.3	90.5	3.5

*In addition to Si, Ti, and Ca, Al was also detected at a low ratio, which is not presented in this table.

of the paper. This result suggests that HDTMS gas molecules were able to effectively diffuse and react with both sides of the paper (paper thickness ≈ 500 µm), including the front side facing the liquid HDTMS and the back side facing away from it, resulting in comparable hydrophobicity on both surfaces. In this study, the 0.1H sample was selected for further investigation because it required the least amount of HDTMS liquid while exhibiting similar contact angles to the samples prepared with higher HDTMS dosages (0.5H and 1H samples). When HDTMS was combined with TTIP at different concentrations, significant enhancement of hydrophobicity was observed. The TTIP solutions at 10% to 15% v/v markedly increased the contact angles on both sides of the paper, ranging from 150° to 154°, demonstrating a superhydrophobic character on both surfaces (Figure 5(b)).

To investigate the effect of vapor deposition time, the water contact angles of the 0.1H+10T sample treated at different silylation durations were examined (Figure 5(c)). The sample treated for 10 min showed initial contact angles of 141° and 146° for the front and back sides, respectively; however, these angles decreased to 0° within 10 s, indicating incomplete condensation reactions. In contrast, the sample treated for 30 min and 60 min exhibited stable contact angles of approximately 151° on both sides. These results suggest that a vapor deposition time of 30 min is sufficient to achieve a superhydrophobic surface modification. Notably, water droplets could easily roll off the surfaces of the 30 min and 60 min samples, demonstrating excellent water repellency. The droplet base appeared slightly flattened because the blotting paper used in this experiment had coarse fibers and a soft texture, which caused the water droplet base to slightly sink into the paper surface.

The SA or water roll-off angle results are shown in Figure 5(d). The optimal-condition sample, 0.1H+10T treated for 30 min, exhibited an average SA of 4.9°. Combined with its average water contact angle of 151° (see Figure 5(c)), this low SA confirms the superhydrophobic behavior of the treated paper, as a surface is generally considered superhydrophobic when it exhibits a water contact angle greater than 150° and a roll-off angle lower than 10° [38]. Supplementary Videos S1 and S2 further demonstrate the facile roll-off of water droplets from this treated paper surface (see Supplementary Data file). These results are consistent with previous studies on superhydrophobic paper made from different materials. Yang *et al.* fabricated superhydrophobic paper by spray coating with the PDMS/$CaCO_3$ layer, achieving an average water contact angle of 151.1° and an average sliding angle of 9° [39]. Similarly, Kan *et al.* developed cellulose-based superhydrophobic paper by applying the cellulose derivative and SiO_2 nanoparticles, resulting in an average water contact angle of 155° and an average sliding angle of 4.1° [40]

The characteristic change of the inherently hydrophilic blotting paper into a superhydrophobic paper can be attributed to the formation of long hydrocarbon chains from the hexadecyl groups of HDTMS, which covalently bonded to both –TiOH and –OH groups on the cellulose surface. The sprayed TTIP solution acted as both a primer, promoting stronger bonding, and a catalyst facilitating the hydrolysis of TTIP to form –TiOH and its subsequent condensation into –TiOC– (bonded to cellulose) and –TiOSi– (bonded to HDTMS). Upon sufficient reaction time, these reactions generated long alkyl chains and TiO_2 particles forming coating layer on the fiber surface, consistent with the SEM observations in Figure 2(h–j).

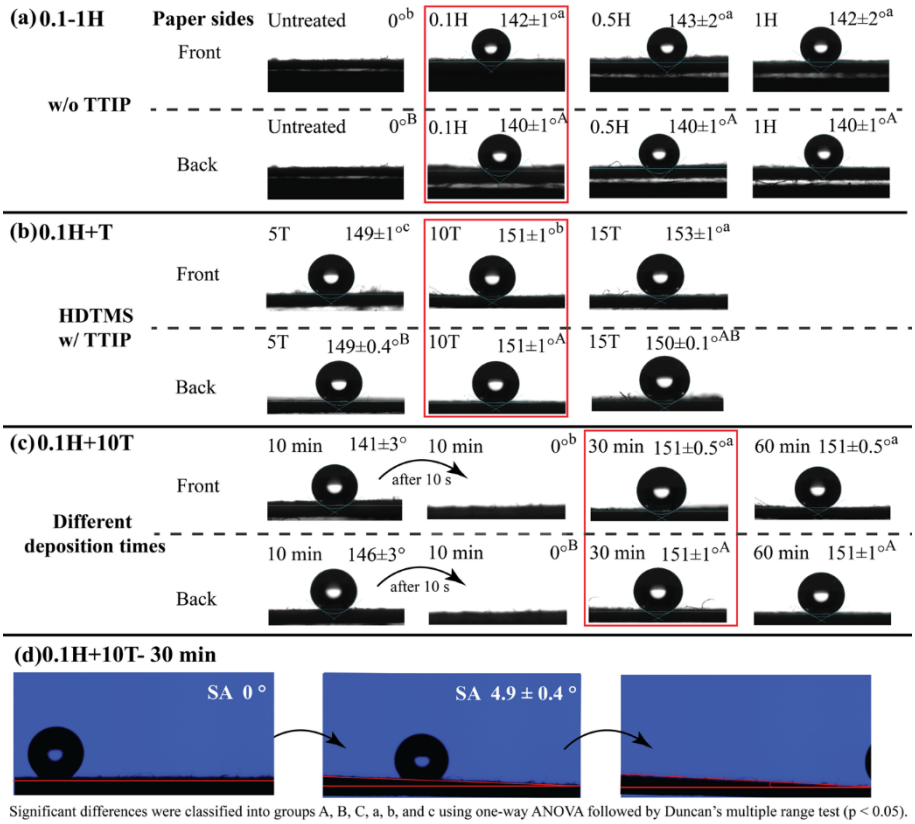


Figure 5. Water contact angles and sliding angle (SA) of untreated and treated paper samples on the front and back sides: (a) different HDTMS liquid amounts, (b) different TTIP concentrations, (c) different vapor deposition times, and (d) SA with sequential water-droplet roll-off images.

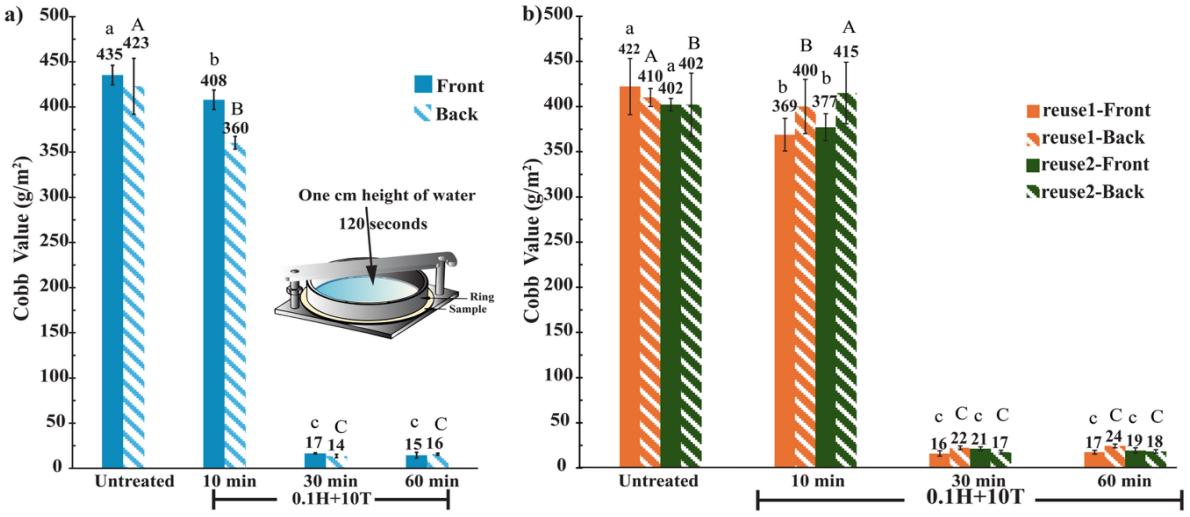
3.4.2 Cobb test

The Cobb test was performed to evaluate the water uptake of the paper samples after 120 s ($Cobb_{120}$) of contact with water. The results for the untreated and 0.1H–10T treated papers at different vapor deposition times are shown in Figure 6. The untreated paper exhibited a high $Cobb_{120}$ value of 435 ± 11 $g{\cdot}m^{-2}$, indicating strong hydrophilicity. This behavior is attributed to the intrinsic absorbent characteristic of blotting paper, which is composed of coarse cellulose fibers with numerous pores and abundant hydroxyl groups, and lacks any hydrophobic modification. After treatment with HDTMS combined with TTIP (the 0.1H–10T sample) for 10 min of vapor deposition, the $Cobb_{120}$ value slightly decreased to 408 ± 11 $g{\cdot}m^{-2}$. In contrast, when the vapor deposition time was extended to 30 min and 60 min, the $Cobb_{120}$ values sharply decreased to 17 ± 0.6 $g{\cdot}m^{-2}$ and 15 ± 3 $g{\cdot}m^{-2}$, respectively, indicating that the gas-phase silylation on cellulose fibers was achieved at these two durations. Both the 30 min and 60 min treated samples showed a dramatic reduction in water penetration into the paper structure after 120 s of immersion, with no significant difference between the two samples. Interestingly, the Cobb values of the treated samples exhibited no significant differences between the front side (the surface exposed to the silane vapor) and the back side (the surface opposite to the vapor deposition) (Figure 6(a)). In addition, reuse tests conducted for up to three cycles, in which the same samples were subjected to the Cobb test, dried, and then retested in subsequent cycles, showed comparable $Cobb_{120}$ values across all reuse rounds (Figure 6(b)), with no significant differences observed between the front and back sides of the treated paper. These findings suggest that a 30 min vapor deposition is sufficient to achieve effective gas-phase silylation, imparting hydrophobic modification to both sides of the blotting paper and enabling reuse after exposure to water.

The Cobb test is considered a bulk measurement, as it involves immersing paper in water under a pressure of 1 cm H_2O to assess its water absorption capacity. The untreated blotting paper exhibited a highly porous structure and abundant hydrophilic hydroxyl groups. After treatment with HDTMS via the chemical vapor deposition method, the HDTMS gas molecules were able to penetrate through the porous network of the paper and react with the hydroxyl groups on individual cellulose fiber surfaces. Compared with a surface coating approach, Ni *et al*. [41] developed a laccase-catalyzed chitosan–monophenol copolymer coating on unbleached kraft paper, which reduced the Cobb value at 5 min from 85.4 $g{\cdot}m^{-2}$ to 48.66 $g{\cdot}m^{-2}$. Another study on superhydrophobic-coated paper by Nan *et al.* [42] reported a bilayer structure composed of a sodium alginate/soy protein isolate base layer and an alkyl ketene dimer/bamboo powder/ carboxycellulose nanofiber top layer, achieving average values of 156.8° for the water contact angle, 16.5° for the sliding angle achieving average values of a water contact angle of 156.8°, a sliding angle of 16.5°, and a $Cobb_{60}$ value (60 s test) of 14.89 $g{\cdot}m^{-2}$. Notably, the gas-phase silylation method employed in the present study resulted in a distinct improvement in hydrophobic performance, reducing the $Cobb_{120}$ value from 435 $g{\cdot}m^{-2}$ to 17 $g{\cdot}m^{-2}$. These findings suggest that HDTMS in the gas phase effectively enhances water resistance within the porous paper structure through a different modification pathway compared to surface coating approaches.

3.4.3 Surface roughness

The Rq values of the untreated paper and the papers treated with 0.1H and 0.1H–10T (30-min deposition time) were 17.1 ± 2.2, 16.8 ± 2.5, and 22.0 ± 2.5 nm, respectively (see AFM images in Figure 7). The comparable Rq values of the untreated and 0.1H samples indicate that HDTMS treatment did not markedly alter the surface roughness. Nevertheless, a change in surface topography was clearly observed in Figure 7(b), where the modified surface appeared to have a different texture compared with the untreated paper (Figure 7(a)). According to the contact angle results, the enhanced hydrophobicity of 0.1H sample was mainly attributed to the reduced surface energy imparted by the low-polarity alkyl chains of HDTMS. In contrast, the significantly higher Rq of 0.1H–10T sample was associated with the formation of small particles of Ti-derived structures from cross-linked TTIP itself and TTIP-linked HDTMS, together with the presence of the low-polarity alkyl chains of HDTMS.



Significant differences were classified into groups A, B, C, a, b, and c using one-way ANOVA followed by Duncan's multiple range test ($p < 0.05$).

Figure 6. $Cobb_{120}$ values of untreated and treated paper samples at different deposition time:(a) original front and back and (b) reuse front and back.

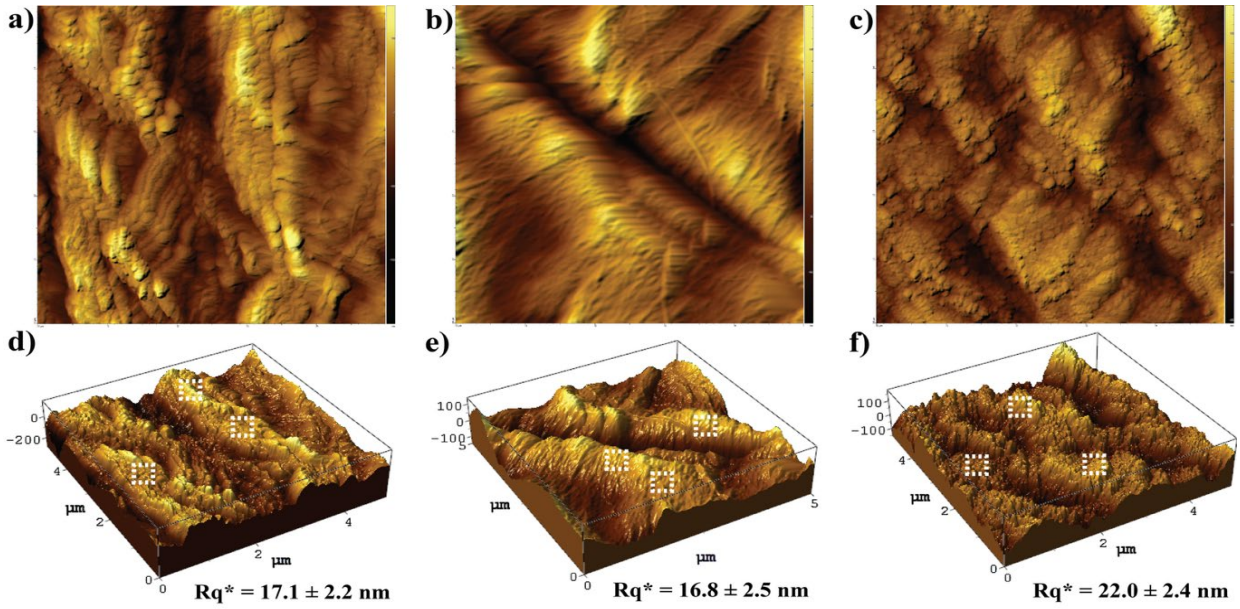


Figure 7. AFM images and surface roughness of (a, d) untreated paper, (b, e) 0.1H-treated paper, and (c, f) 0.1H–10T-treated paper.

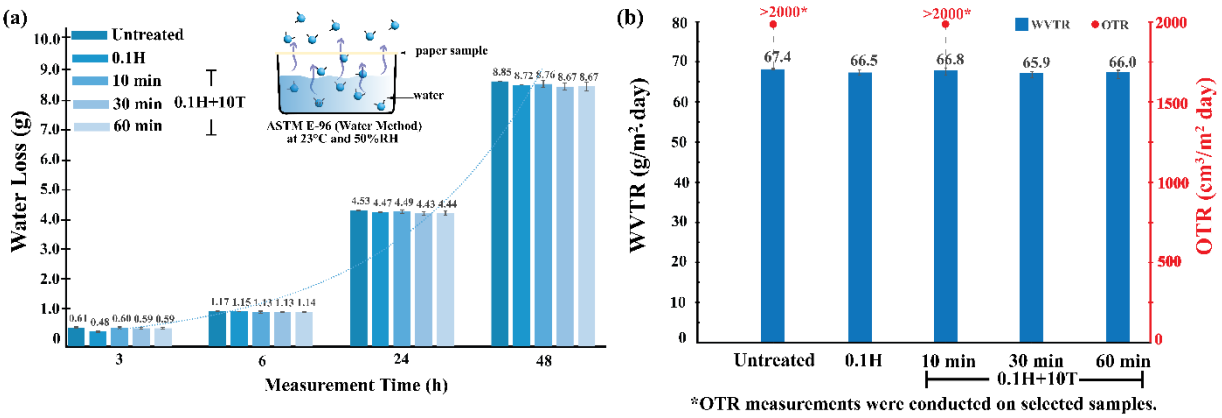


Figure 8. Gas permeability using (a) water loss from WVTR cup and (b) water vapor and oxygen transmission rates of untreated and treated paper samples at different deposition times.

According to Wenzel's contact angle theory, surface hydrophobicity can be enhanced by both decreasing the surface energy and increasing the micro-/nanoscale roughness of the hydrophobic surface [32]. Therefore, the superior hydrophobicity of the 0.1H–10T sample resulted from the combined effects of low surface free energy and increased nanoscale roughness. The increase in surface roughness after modification is consistent with previous observations for polymer-modified cellulosic substrates. Kaja *et al.* reported that polyethylene coating increased the Rq of cotton textile from approximately 0.185 μm to 0.439 μm, indicating that surface deposition can substantially alter the surface topography of cellulose-based materials [43].

3.4.4 Water vapor and oxygen transmission rates

The water vapor transmission test was conducted to evaluate the permeability of water vapor through the paper samples using the cup method. In this method, water was sealed inside a cup, and vapor was allowed to diffuse through the paper under controlled conditions of 23 ± 1.0°C and 50 ± 2.0% relative humidity. As shown in Figure 8(a), the amount of water vapor transmitted increased with time for all samples. The water loss from the cups was comparable between the untreated and treated papers. After 24 h, the calculated WVTR values for the untreated, 0.1H, and 0.1H–10T paper samples treated for 10 min, 30 min, and 60 min were 67.4 $g \cdot m^{-2}$, 66.5 $g \cdot m^{-2}$, 66.8 $g \cdot m^{-2}$, 65.9 $g \cdot m^{-2}$, and 66.0 $g \cdot m^{-2} \cdot$day, respectively (Figure 8(b)). These results showed no significant differences among the samples, indicating that the paper modification did not notably affect water vapor transmission. This result was attributed to the HDTMS gas molecules that reacted directly with the hydroxyl groups on the cellulose fiber surfaces without forming a continuous film layer, thereby preserving the porous structure of the paper. Since the WVTR test involves the diffusion of water in the vapor phase, water vapor can still penetrate through the inter-fiber voids, resulting in similarly high WVTR values comparable to that of the untreated paper. The OTR results exhibited a similar trend to that observed for the WVTR results, as oxygen gas could be readily transmitted through the 0.1H–10T paper samples. The OTR

exceeded the instrument detection limit (>2,000 $cm^3 \cdot m^{-2} \cdot day^{-1}$) (Figure 8(b)), indicating that oxygen could readily permeate through the treated paper. This implies that the treated paper retained high gas permeability rather than acting as an oxygen barrier. Furthermore, the presence of TTIP did not significantly increase vapor barrier properties or close the surface pores (Figure 2(i–n)), which show that the paper surface retained its porous morphology allowing vapor diffusion.

The modified paper developed in this study exhibited effective water resistance while maintaining air permeability. Such water-repellent yet breathable characteristics are advantageous in various fields, for example, (i) textile applications, where materials must block liquid water but allow vapor and heat transfer for outdoor or protective clothing [44]; (ii) medical uses, where breathable liquid barriers help prevent microbial contamination while maintaining air exchange, as demonstrated in a previous study, a waterproof–breathable hemp/cotton hydroentangled nonwoven was developed through surface modification with silica–polyvinylsilsesquioxane [45]; and (iii) fresh produce packaging, where hydrophobic yet vapour-permeable paper materials enable moisture and gas exchange from fresh-cut fruits and vegetables, thereby supporting respiration and extending shelf life [46].

3.5 Color

The untreated and treated papers exhibited Lab* color values, as shown in Figure 9a. The L* value represents lightness, the a* value corresponds to the red–green coordinate, and the b* value indicates the yellow–blue coordinate along the positive and negative axes, respectively. The experimental results revealed that the L* values showed no significant differences among all treatment conditions, ranging from 94 to 95. This trend was consistent with the a* values, which were also similar for all samples. However, when comparing the b* values representing the yellow–blue coordinate, the untreated paper showed a value of 3.1. After treatment, the b* values increased toward the yellow axis. The 0.1H sample exhibited a slight increase to 4.8, while the HDTMS-treated samples incorporated with 10% v/v TTIP solution showed a significant increase in the b* values with longer silylation times at 10 min, 30 min, and 60 min, reaching 5.1, 6.6, and 8.0, respectively.

Figure 9(b) shows the color difference (ΔE*) between the untreated and treated paper samples. The 0.1H sample exhibited an avergae ΔE* value of 1.8. When HDTMS incorporated with a 10% v/v TTIP solution for 10 min, 30 min, and 60 min silylation times, the average ΔE* values of the treated papers increased to 2.0, 3.6, and 5.3, respectively. According to color difference theory, a ΔE* value ≤ 2 is considered perceptible only upon close observation, but not noticeable at a glance. Therefore, the samples treated with 0.1H and 0.1H–10T for 10 min showed minimal color variation compared to the untreated paper, which is hardly distinguishable to the human eye. However, as the silylation time increased (30 and 60 min), the color difference became more pronounced. This observation is consistent with the increased b* values, indicating that the paper appeared more yellow to the naked eye. The increased yellowness was mainly attributed to the presence of TTIP, suggesting that further studies should focus on reducing the amount of TTIP in combination with other process parameters to minimize the color difference. This adjustment would be particularly beneficial for applications that require maintaining the whiteness of the paper.

3.6 Stability and durability of the treated sample

The long-term storage stability of the treated paper is shown in Figure 10(a). The water contact angles of the untreated, 0.1H, and 0.1H–10T (30 min vapor deposition time) samples remained close to their initial values after 7 months of storage at room temperature and 30 ± 5% RH, with no significant differences (ns, $p > 0.05$). This indicates that TTIP-assisted HDTMS vapor deposition provided stable hydrophobicity during prolonged storage. The environmental stability of the 0.1H–10T sample was further evaluated under different conditions, including freezing at −18°C, heating at 90°C, and steam exposure. The water contact angle was measured immediately after 2 h of exposure to each condition and compared with that of the sample maintained under ambient conditions (Figure 10(b)). No significant changes in water contact angle were observed compared with the ambient condition, demonstrating good stability under different temperature and humidity conditions and supporting its potential for packaging applications.

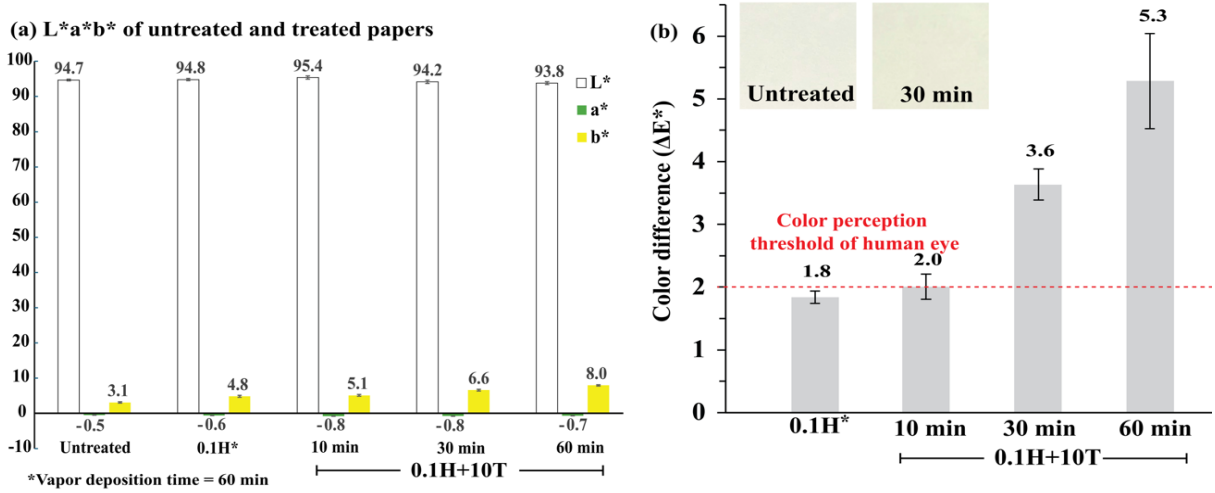
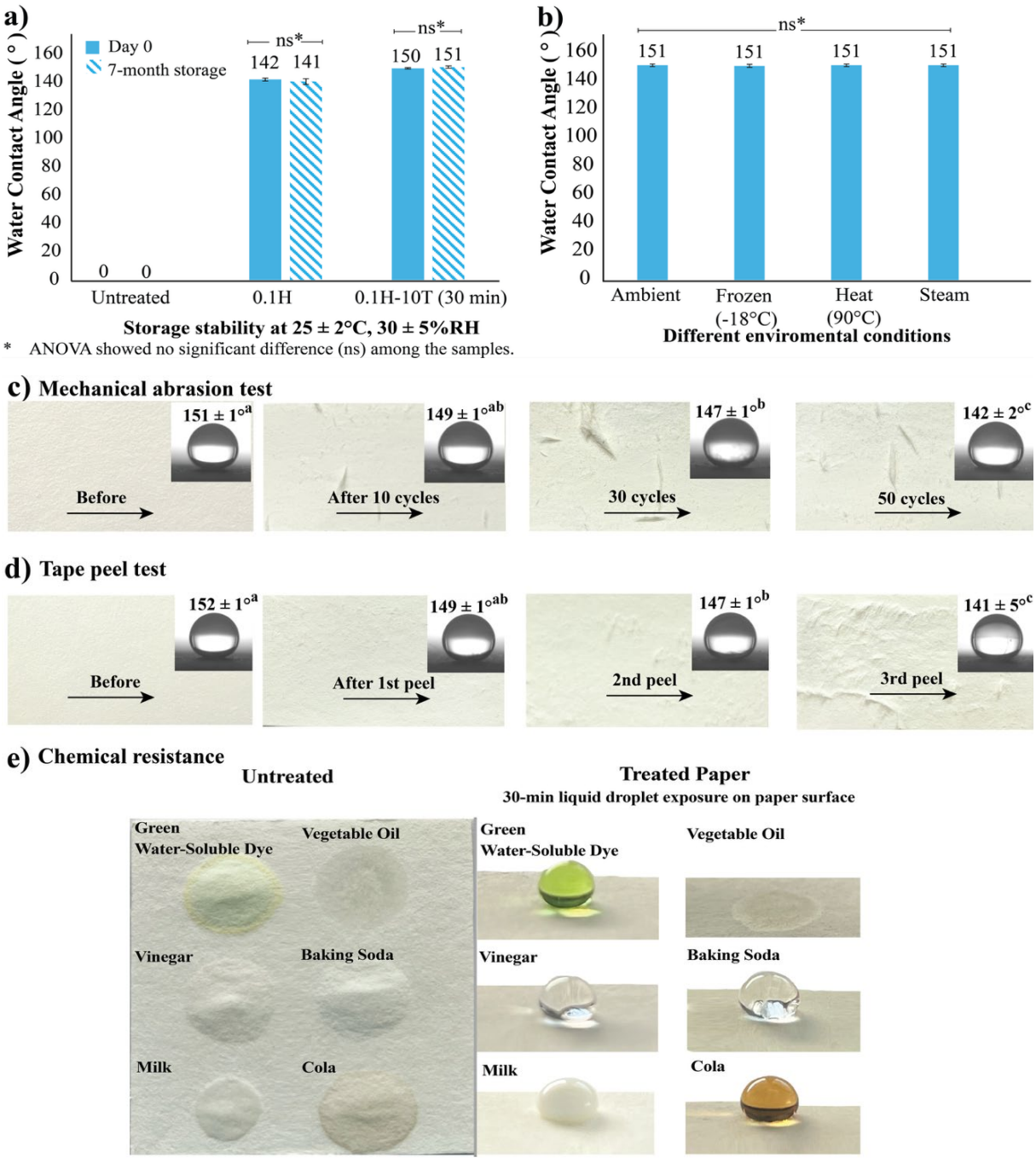


Figure 9. CIELAB Color of paper samples: (a) L*a*b* values and (b) color difference between untreated and treated papers.



Significant differences were classified into groups a, b, and c using one-way ANOVA followed by Duncan's multiple range test ($p < 0.05$).

Figure 10. Stability and durability of the treated paper: (a) long-term storage, (b) storage under different environmental conditions, (c) mechanical abrasion, (d) tape peeling, and (e) household chemical resistance.

The mechanical durability of the treated paper was evaluated using mechanical abrasion and tape-peel tests, as shown in Figure 10 (c–d), respectively. The water contact angle decreased slightly with increasing abrasion and peeling cycles, likely due to the gradual removal of the modified rough surface associated with TiO_2 particle formation. Nevertheless, the exposed underlying surfaces remained hydrophobic, suggesting that gaseous HDTMS diffused into the porous paper fiber network during CVD rather than modifying only the outermost surface.

The resistance to household chemicals is shown in Figure 10(e). Untreated paper rapidly absorbed all tested liquids, whereas the treated paper resisted penetration by green water-soluble dye, vinegar (pH 2), baking soda solution (pH 9), milk, and cola for 30 min. No penetration stains remained after wiping the dye, vinegar, and baking soda solution off, while sticky residues from milk and cola could be removed with a moistened cotton cloth. In contrast, vegetable oil readily wetted and penetrated the treated paper because of the nonpolar nature of the modified surface. This behavior is consistent with the "like dissolves like" principle and with Cai *et al.* [47], who reported rapid diesel-oil permeation through hydrophobic HDTMS–TiO_2-coated stainless-steel mesh while water was retained.

3.7 Potential for practical applications

Compared with conventional liquid-phase silane treatments, such as sol–gel dip coating or roll coating, the present CVD approach avoids direct solvent contact and requires only a very small amount of silane, suggesting potential reductions in material costs. Liquid-phase methods generally involve larger volumes of silane and solvent, immersion steps, and subsequent drying, which increase reagent consumption and processing requirements; moreover, solvent wetting and drying may lead to non-uniform coatings or substrate warping. A detailed comparison between liquid-phase coating and CVD is provided in Table S2 in the Supplementary Data.

The translation of the CVD laboratory-scale process to continuous industrial production would require additional engineering development. A feasible scale-up concept would be to integrate the silylation step into a continuous roll-to-roll paper finishing line by introducing a closed vapor-deposition chamber into the existing production system. This would be similar to industrial vacuum metallization, where the paper or flexible web is continuously unwound, passes through a closed and pressure-controlled deposition chamber, and is then rewound. The main challenges are (i) reducing the CVD residence time to maintain a high production speed and (ii) obtaining uniform HDTMS vapor exposure across the full paper width and on both sides of the sheet. Chamber pressure could be further optimized because it can affect vapor transport, deposition rate, and coating uniformity. For large-scale production, an inert carrier gas such as N_2 could be used to distribute HDTMS vapor more evenly through gas manifolds, gas rings, or showerhead-type inlets placed on both sides of the moving paper web. Similar controlled gas-delivery systems have been used for organosilane treatment of cellulose (1), and optimized showerhead systems have been shown to improve deposition uniformity in CVD processes [48,49].

Regarding toxicity and environmental impact, HDTMS is a widely studied silane that is fluorine-free, food-safe, and environmentally friendly. HDTMS-modified paper has shown satisfactory bio-compatibility (>80% L929 cell viability), while TiO_2-based packaging systems have demonstrated negligible titanium migration and non-cytotoxic leachates [50,51]. After hydrolysis and condensation, HDTMS and TTIP are converted from reactive liquid precursors into a more stable inorganic–organic network on the paper surface, substantially reducing their volatility and potential leaching compared with the unreacted chemicals. Nevertheless, the modified paper is not fully biodegradable because of the incorporated siloxane/titania phase. Therefore, end-of-life management should preferably focus on paper recycling, where repulping may facilitate the separation of the condensed HDTMS–TTIP phase from the cellulose fibers. The efficiency of this separation should be further investigated in future work.

4. Conclusions

This study proposed a method to enhance the water resistance of paper through chemical vapor deposition using gas-phase silylation of HDTMS combined with a TTIP catalyst. The aim was to identify the optimal conditions and ratio of HDTMS and TTIP required to create a superhydrophobic surface on highly absorbent paper. The results revealed that treating paper samples (36 cm^2) with 0.1 mL of HDTMS (equivalent to 28 $mL \cdot m^{-2}$) together with spraying a 10% v/v TTIP solution as a catalytic primer significantly improved the bonding of HDTMS molecules to the cellulose fiber surface during gas-phase silylation. A reaction time of 30 min yielded the optimal water resistance in both surface and bulk properties. The HDTMS vapor molecules were able to penetrate the paper matrix, forming a superhydrophobic surface on both sides, including the one not directly exposed to the HDTMS liquid. As a result, the water contact angle increased from 0° (untreated blotting paper) to between 150° and 154°. Furthermore, the Cobb value, which evaluates water uptake based on bulk absorption, decreased dramatically from 435 $g \cdot m^{-2}$ to 17 $g \cdot m^{-2}$ on both sides of the paper. Meanwhile, the treated papers maintained good breathability, as confirmed by WVTR values of 66 $g \cdot m^{-2}$ to 67 $g \cdot m^{-2} \cdot day$ and OTR more than 2,000 $cm^3 \cdot m^{-2} \cdot day^{-1}$ comparable to those of untreated samples. These findings demonstrate potential for extending this technique to the development of breathable waterproof paper materials for medical and healthcare applications, such as wound dressings and wearable products, as well as for fresh produce packaging to prolong the shelf life of fruits and vegetables.

Declaration of competing interest

The authors declare that they have no known competing financial interests or personal relationships that could have appeared to influence the work reported in this paper.

Ethical statement

This study involved no human or animal subjects and raised no ethical concerns.

Acknowledgments

This research was financially supported by the Sci Re-engagement Fund, Faculty of Science, Chulalongkorn University, with additional financial support from the Pulp, Paper and Packaging Technology Program, Faculty of Science, Chulalongkorn University. The authors gratefully acknowledge the Department of Imaging and Printing Technology, Faculty of Science, Chulalongkorn University, for providing the facilities and equipment necessary for this research.

References

[1] M. Mujtaba, J. Lipponen, M. Ojanen, S. Puttonen, and H. Vaittinen, "Trends and challenges in the development of bio-based barrier coating materials for paper/cardboard food packaging: A review," *Science of The Total Environment,* vol. 851, no. 2, p. 158328, 2022.

[2] N. Cai, S. Jia, K. Sun, J. Zhu, C. Zhao, and H. Yang, "High-value utilization of waste plastics: Transforming plastic polymers into thin-walled and uniform carbon nanotubes via catalytic pyrolysis," *Green Energy & Environment*, in press, 2025.

[3] E. Shlush, and M. Davidovich-Pinhas, "Bioplastics for food packaging," *Trends in Food Science & Technology,* vol. 125, pp. 66–80, 2022.

[4] Z.-Q. Tan, T. Kobayashi, and D. Aht-Ong, "Extraction of cellulose nanofibers from empty palm fruit bunches via mechanical defibrillation," *Journal of Metals, Materials and Minerals,* vol. 31, no. 3, pp. 10–19, 2021.

[5] S. Basak, M. S. Dangate, and S. Samy, "Oil- and water-resistant paper coatings: A review," *Progress in Organic Coatings,* vol. 186, p. 107938, 2024.

[6] P. Piltonen, P. Karinkanta, and J. Niinimäki, "The effect of styrene–butadiene latex carboxylation on adhesion," *International Journal of Adhesion and Adhesives,* vol. 54, pp. 82–85, 2014.

[7] Y. Du, J. Liu, B. Wang, H. Li, and Y. Su, "The influence of starch-based bio-latex on microstructure and surface properties of paper coating," *Progress in Organic Coatings,* vol. 116, pp. 51–56, 2018.

[8] E. Basiak, A. Lenart, and F. Debeaufort, "How glycerol and water contents affect the structural and functional properties of starch-based edible films," *Polymers,* vol. 10, no. 4, p. 412, 2018.

[9] A. d. A. d. Santos, L. C. Matos., M. C. Mendonça, R. C. d. Lago, M. C. d. S. Muguet, R. A. P. Damásio, A. Ponzecchi, J. R. Soares, A. R. Sanadi, and G. H. D. Tonoli, "Evaluation of paper coated with cationic starch and carnauba wax mixtures regarding barrier properties," *Industrial Crops and Products,* vol. 203, p. 117177, 2023.

[10] X. Jing, X. Li, Y. Jiang, R. Zhao, Q. Ding, and W. Han, "Excellent coating of collagen fiber/chitosan-based materials that is water- and oil-resistant and fluorine-free," *Carbohydrate Polymers,* vol. 266, p. 118173, 2021.

[11] Z. Wang, W. Kong, L. Si, J. Niu, Y. Liu, L. Yin, and Z.Tian, "Robust and thermally stable butterfly-like $Co(OH)_2$/hexadecyl trimethoxysilane superhydrophobic mesh filters prepared by electrodeposition for highly efficient oil/water separation," *Industrial & Engineering Chemistry Research,* vol. 58, no. 22, pp. 9576–9584, 2019.

[12] M. Seth, H. Khan, and S. Jana, "Hierarchically structured alpha-nickel hydroxide based superhydrophobic and antibacterial coating on cellulosic materials for oil-water separation," *Materials Chemistry and Physics,* vol. 249, p. 123030, 2020.

[13] N. Ahmad, S. Rasheed, K. Ahmed, S. G. Musharraf, M. Najam-ul-Haq, and D. Hussain, "Facile two-step functionalization of multifunctional superhydrophobic cotton fabric for UV-blocking, self cleaning, antibacterial, and oil-water separation," *Separation and Purification Technology,* vol. 306, p. 122626, 2023.

[14] R. R. R. Prieto and M. U. Herrera, "Coating of zinc substrates with fluorosilane molecules using a water-treatment technique as a pre-coating procedure for the creation of superhydrophobic surfaces," *Journal of Metals, Materials and Minerals,* vol. 35, no. 4, p. e2217, 2025.

[15] K. K. Gleason, "CVD Polymers: Fabrication of Organic Surfaces and Devices, 1st ed. Weinheim, Germany: Wiley-VCH, p. 461 2015.

[16] P. S. Goh, R. Naim, M. Rahbari-Sisakht, and A. F. Ismail, "Modification of membrane hydrophobicity in membrane contactors for environmental remediation," *Separation and Purification Technology,* vol. 227, p. 115721, 2019.

[17] H. Şakalak, K. Yılmaz, M. Gürsoy, and M. Karaman, "Roll-to roll initiated chemical vapor deposition of super hydrophobic thin films on large-scale flexible substrates," *Chemical Engineering Science,* vol. 215, p. 115466, 2020.

[18] F. Rafieian, M. Hosseini, M. Jonoobi, and Q. Yu, "Development of hydrophobic nanocellulose-based aerogel via chemical vapor deposition for oil separation for water treatment," *Cellulose,* vol. 25, no. 8, pp. 4695–4710, 2018.

[19] D. Yue, Q. Feng, X. Huang, X. Zhang, and H. Chen, "In situ fabrication of a superhydrophobic ORMOSIL coating on wood by an ammonia–HMDS vapor treatment," *Coatings*, vol. 9, no. 9, p. 556, 2019.

[20] X. Cao, X. Guo , T. Xiao, W. Jia, X. Liu, C. Li, H. Zhang, P. Fatehi, and H. Shi, "Superhydrophobic biomass-based aerogel fabricated in lithium bromide trihydrate for oil adsorption," *Separation and Purification Technology,* vol. 354, p. 129421, 2025.

[21] L. Yu, Z. Zhang, H. Tang, and J. Zhou, "Fabrication of hydrophobic cellulosic materials via gas–solid silylation reaction for oil/water separation," *Cellulose,* vol. 26, no. 6, pp. 4021–4037, 2019.

[22] A. De Santis, G. Nicastro, L. Riva, A. Sacchetti, D. Ghirardello, and C. Punta, "Cellulose nanofibers for grease and air barrier properties enhancement: A comparison on recycled and food contact paper samples," *Carbohydrate Polymers,* vol. 368, p. 124237, 2025.

[23] A. Mathew, A. Poulose, A. Peter, H. M. Lal, A. Uthaman, M. S. M. Saheed, D. Pasquini, Y. Grohens, D. A. Gopakumar, and J. Ja. George, "Bio-inspired hydrophobicity in cellulose nanopaper via thermal-induced phase separation of beeswax: A new strategy to develop sustainable food packaging materials and its service life prediction," *Food Packaging and Shelf Life,* vol. 48, p. 101461, 2025.

[24] O. E. Pecho, R. Ghinea, R. Alessandretti, M. M. Pérez, and A. Della Bona, "Visual and instrumental shade matching using CIELAB and CIEDE2000 color difference formulas," *Dental Materials,* vol. 32, no. 1, pp. 82–92, 2016.

[25] C. Magdaleno-López, and J. de Jesús Pérez-Bueno, "Quantitative evaluation for the ASTM D4541-17/D7234 and ASTM D3359 adhesion norms with digital optical microscopy for surface modifications with flame and APPJ," *International Journal of Adhesion and Adhesives,* vol. 98, p. 102551, 2020.

[26] L. Sun, K. Fang, W. Chen, K. Liu, J. Zhu, and C. Zhang, "Fabrication of a novel superhydrophobic cotton by HDTMS with TiO_2 supported activated carbon nanocomposites for photo-catalysis and oil/water separation," *Industrial Crops and Products,* vol. 189, p. 115836, 2022.

[27] F. Gubbels, "An overview of the chemistry of condensation curing silicone sealants and adhesives," *International Journal of Adhesion and Adhesives,* vol. 132, p. 103728, 2024.

[28] Y. Paz, "Self-assembled monolayers and titanium dioxide: From surface patterning to potential applications," *Beilstein Journal of Nanotechnology,* vol. 2, pp. 845–861, 2011.

[29] M. F. Nsib, F. Hajji, A. Mayoufi, N. Moussa, A. Rayes, and A. Houas, "In situ synthesis and characterization of TiO_2/HPM

cellulose hybrid material for the photocatalytic degradation of 4-NP under visible light," *Comptes Rendus. Chimie,* vol. 17, no. 7-8, pp. 839–848, 2014.

[30] M. Castellano, A. Gandini, P. Fabbri, and M. N. Belgacem, "Modification of cellulose fibres with organosilanes: Under what conditions does coupling occur?," *Journal of Colloid and Interface Science,* vol. 273, no. 2, pp. 505–511, 2004.

[31] M. M. Rashid, B. Simončič, M. Zorc, R. Fink, N. Č. Korošin, A. Šuligoj, J. Kovač, I.Jerman, and B. Tomšič, "Synthesis of a new amino/phosphate-modified TiO_2/rGO hybrid nanocomposite for sustainable textile functionalization," *Journal of Environmental Chemical Engineering,* vol. 13, no. 3, p. 116555, 2025.

[32] K. Pacaphol, K. Seraypheap, and D. Aht-Ong, "Extraction and silylation of cellulose nanofibers from agricultural bamboo leaf waste for hydrophobic coating on paper," *Journal of Natural Fibers,* vol. 20, no. 1, p. 2178581, 2023.

[33] S. Habibi, and M. Jamshidi, "Synthesis of TiO_2 nanoparticles coated on cellulose nanofibers with different morphologies: Effect of the template and sol-gel parameters," *Materials Science in Semiconductor Processing,* vol. 109, p. 104927, 2020.

[34] P. Thummanukitcharoen, S. Limpanart, and K. Srikulkit, "Preparation of organosilane treated microcrystalline (SiMCC) and SiMCC/ polypropylene composites", *Journal of Metals, Materials and Minerals*, vol. 22, no. 1, 2012,

[35] J. Ou, F. Wang, W. Li, M. Yan, and A. Amirfazli, "Methyltrimethoxysilane as a multipurpose chemical for durable superhydrophobic cotton fabric," *Progress in Organic Coatings,* vol. 146, p. 105700, 2020.

[36] S. Bhol, N. C. Sahu, S. G. Mohanty, V. R. Maddala, B. K. Panigrahi, and P. Bhosale, "A top-electrode-based liquid-solid triboelectric nanogenerator for energy harvesting and ethanol detection," *Journal of Metals, Materials and Minerals,* vol. 36, no. 1, p. e2600, 2026.

[37] L. Zhang, Y. Liu, X. Wang, D. Chen, and H. Ding, "Fabrication of sericite-TiO_2/HDTMS superhydrophobic self-cleaning coatings by hydrothermal method," *Journal of Alloys and Compounds,* vol. 1014, p. 178677, 2025.

[38] M. Z. Khan, J. Militky, M. Petru, B. Tomková, A. Ali, E. Tören, and S. Perveen, "Recent advances in superhydrophobic surfaces for practical applications: A review," *European Polymer Journal,* vol. 178, p. 111481, 2022.

[39] J. Yang, Y. He, F. Sun, P. Zhu, Y. Wu, L. Peng, and H. Li, "Preparation of superhydrophobic and antibacterial paper-based piezoresistive pressure sensor for human motion detection," *Applied Surface Science,* vol. 714, p. 164475, 2025.

[40] L. Kan, X. Zhang, Q. Huang, Y. Wang, M. Tian, Q. Huang, W. Wei, F. Zhang, and X. Wang, "Fabrication of cellulose-based and fluorine/silane free superhydrophobic paper by a green and sustainable approach," *Industrial Crops and Products,* vol. 203, p. 117226, 2023.

[41] S. Ni, N. Liu, Y. Fu, H. Bian, Y. Zhang, X. Chen, H. Gao, and H. Dai, "Laccase-catalyzed chitosan-monophenol copolymer as a coating on paper enhances its hydrophobicity and strength," *Progress in Organic Coatings,* vol. 151, p. 106026, 2021.

[42] H. Nan, L. Wei, W. Zhang, H. Sun, H. Zhou, J. Ma, and Z. Zhan, "Development of fluorine-free, all-water-based bilayer-coated paper with superhydrophobicity, oil resistance, and anti-bacterial adhesion properties for high-performance food packaging," *Food Bioscience,* vol. 75, p. 108199, 2026.

[43] K. R. Kaja, S. Hajra, S. Panda, M. Belal, S. Nam, P. Pakawanit, B. K. Panigrahi, H. Khanbareh, C. Bowen, J. Yu, and H. J. Kim, "Waste polyethylene-coated fabrics for dual-mode interfaces triboelectrification for self-powered sensors," *Results in Engineering,* vol. 28, p. 107111, 2025.

[44] S. K. Fleetwood, M. Kleiman, V. French, J. Kaschuk, and E. J. Foster, "Bioinspired waterproof, breathable materials: How does nature transport water across its surfaces and through its membranes?," *Progress in Materials Science,* vol. 156, p. 101578, 2026.

[45] H. Gao, W. Sun, C. Wang, M. Jing, L. Yang, H. Gao, and R. Zhao, "Improving waterproof-breathable capability of degradable macroporous film/hemp hydroentangled nonwovens composite membranes by porous structure and surface wettability modification," *Colloids and Surfaces A: Physicochemical and Engineering Aspects,* vol. 674, p. 131963, 2023.

[46] P. V. Rodrigues, M. C. R. Castro, A. M. S. Soares, L. Melro, and A. V. Machado, "Development of a polyethylene breathable packaging film with modified microcrystalline cellulose for fresh products," *Macromol,* vol. 4, no. 2, pp. 269–281, 2024.

[47] Y. Cai, Q. Zhao, X. Quan, W. Feng, and Q. Wang, "Fluorine-free and hydrophobic hexadecyltrimethoxysilane-TiO_2 coated mesh for gravity-driven oil/water separation," *Colloids and Surfaces A: Physicochemical and Engineering Aspects,* vol. 586, p. 124189, 2020.

[48] P. Cerny, P. Bartos, P. Kriz, P. Olsan, and P. Spatenka, "Highly hydrophobic organosilane-functionalized cellulose: A promising filler for thermoplastic composites," *Materials,* vol. 14, no. 8, p. 14082005, 2021.

[49] Q. Li, Y. Zhang, B. Ji, S. Zhang, and R. Tu, "Improvement of SiC deposition uniformity in CVD reactor by showerhead with baffle," *Journal of Crystal Growth,* vol. 615, p. 127255, 2023.

[50] Y. He, Y. Zhou, J. Cai, Y. Feng, B. Luo, and M. Liu, "Facile fabrication of hydrophobic paper by HDTMS modified chitin nanocrystals coating for food packaging," *Food Hydrocolloids,* vol. 133, p. 107915, 2022.

[51] D. Enescu, A. Dehelean, C. Gonçalves, M. Cerqueira, D. Măgdaș, P. Fuciños, and L. Pastrana, "Evaluation of the specific migration according to EU standards of titanium from Chitosan/Metal complexes films containing TiO_2 particles into different food simulants. A comparative study of the nano-sized vs micro-sized particles," *Food Packaging and Shelf Life,* vol. 26, p. 100579, 2020.